SHOCK PROPAGATION THROUGH GAS WITH DENSITY INHOMOGENEITIES

P.YU. GEORGIEVSKIY[1], V.A. LEVIN[2], O.G. SUTYRIN[1,c]

[1]Institute for Mechanics of Moscow State University, Moscow, 119192, Russia
[2]Institute for Automation and Control Processes of Russian Academy of Sciences, Vladivostok, 690041, Russia
[c]Corresponding author: Tel.: +74959395977; Email: sutyrin@imec.msu.ru

KEYWORDS: **shock propagation, shock interaction, shock refraction, inhomogeneous gas, cumulation**

ABSTRACT: Propagation of a plane shock through non-uniform inviscid gas is numerically investigated. Several types of inhomogeneities – quarter-plane, thin layer, wedge or elliptic bubble filled with high- or low-density gas – are considered. Distinct regular and irregular flow structures are observed and analyzed. New quantitative features of shock-inhomogeneity interactions, such as formation of high-enthalpy wave-structured stream and lamellar vortex are found. Semi-analytical main flow parameters assessment method is proposed. Nearly self-similar growth of well-known "precursor", for interaction of a shock with thin heated layer, is found to be disturbed at late times due to internal "flow choking" process. New quantitative features of shock/gas wedge interaction are found, including a forerunner-like structure for very thin light wedge. The effect of secondary shocks cumulation is revealed for interaction of a shock with both light- and heavy-gas elliptic bubbles. Dependant on bubble geometry and shock properties, different regimes of cumulation – external, internal and transitional – are found. The quantitative dependence of cumulating gas parameters on bubble geometry is investigated.

Interaction of shock waves with high- and low-density gas areas is widely studied in connection with applications in combustion and detonation, supersonic flow-over-body control, supersonic air inlets design. A formation of "forerunner" – wide-scale shock structure, which leaves initial shock behind – is described by in [1] for a problem of shock propagation along heated wall; observed forerunner growth is supposedly self-similar. Empirical classification of regular and irregular shock refractions at oblique slow-fast and fast-slow gas interfaces is given in [2-3]. A broad problem set for shock propagation in heterogeneous and relaxing gases is considered in. [4]; in particular, the authors denote resemblance of propagation of a shock through area of heated or relaxing gases. A propagation of a shock through spherical area of heated gas ("thermic") is studied in [5]; formation of hanging shock near thermic edge and an effect of front straightening after shock moved off thermic are described. Detailed review of interaction of a shock with spherical gas bubbles problems is given in [6,7]. At the moment there are lot of detailed results on such attendant phenomena as bubble distortion, vortex formation and development. Additionally, an effect of shock cumulation at flow symmetry axis has been denoted in [5,8,9], though modest computing means at the time have rendered detailed study of the phenomenon impossible.

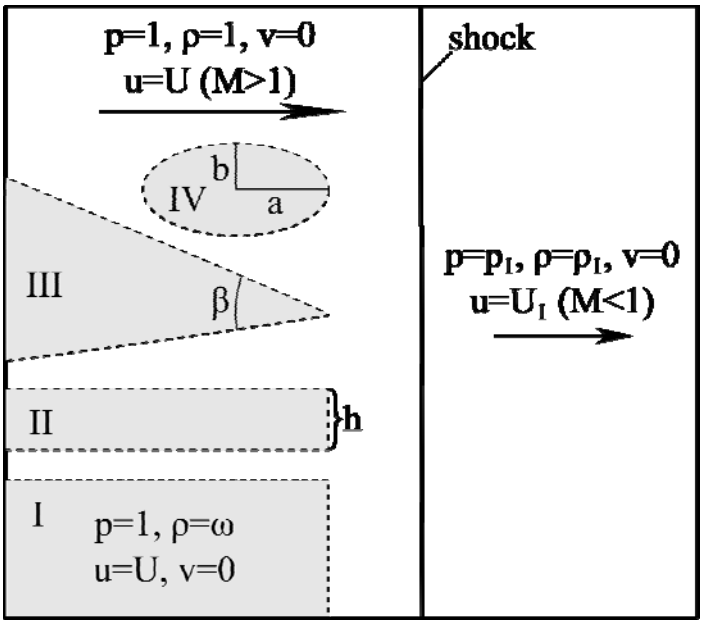

Fig. 1 Four inhomogeneity types shock interacts with: quarter-plane I, thin layer II, wedge III and elliptic bubble IV. The motion is relative to the shock: intensity of the shock determines oncoming flow velocity.

The present paper is devoted to numerical study of a set of plane and axisymmetric problems of shock interaction with local and extensive gas density inhomogeneities. Four geometric inhomogeneity configurations of are considered (fig. 1): quarter-plane I, thin layer II, wedge III and elliptic bubble IV. Some flow features for the cases I and IV are described in earlier works [10-11].

MATEMATICAL AND NUMERICAL MODEL Euler's model of inviscid gas is used to model unsteady two-dimensional plane and axisymmetric flows:

$$\frac{\partial}{\partial t}\begin{pmatrix}\rho\\ \rho u\\ \rho v\\ e\end{pmatrix}+\frac{\partial}{\partial x}\begin{pmatrix}\rho u\\ p+\rho u^2\\ \rho uv\\ (e+p)u\end{pmatrix}+\frac{\partial}{\partial r}\begin{pmatrix}\rho v\\ \rho uv\\ p+\rho v^2\\ (e+p)v\end{pmatrix}=0 \quad \text{(plane flow)}$$

$$\frac{\partial}{\partial t}\begin{pmatrix}\rho\\ \rho u\\ \rho v\\ e\end{pmatrix}+\frac{\partial}{\partial x}\begin{pmatrix}\rho u\\ p+\rho u^2\\ \rho uv\\ (e+p)u\end{pmatrix}+\frac{\partial}{\partial r}\begin{pmatrix}\rho v\\ \rho uv\\ p+\rho v^2\\ (e+p)v\end{pmatrix}=\begin{pmatrix}-\rho v/r\\ -\rho uv/r\\ -\rho v^2/r\\ -(e+p)v/r\end{pmatrix} \quad \text{(axisymmetric flow)}$$

The equations are given for dimensionless parameters $p=\tilde{p}/p_\infty$, $\rho=\tilde{\rho}/\rho_\infty$, $u=\tilde{u}\Big/\sqrt{p_\infty/\rho_\infty}$, where $\tilde{p},\tilde{\rho},\tilde{u}$ are physical values. The total energy e of a volume unit for the perfect inviscid gas is determined as follows:

$$e=\frac{p}{\gamma-1}+\rho\frac{u^2+v^2}{2},\quad \gamma=1.4$$

The MacCormack two-step scheme [12] of second order spatial and temporal accuracy is used. In most cases, a uniform rectangular computational grid is used along with three-point "inwards" differential approximation at grid edges, which preserved second order accuracy. For better resolution in certain cases, local two-step grid adaptation was used near axis of symmetry $(r=0)$. An external monotonization method [13] was used to suppress non-physical oscillations near shock surfaces. The stability of the scheme has been controlled by CFL condition.

INTERACTION OF A SHOCK WITH QUARTER-PLANE DENSITY AREA The interaction of a shock with quarter-plane area of high- or low-density gas (I at fig. 1) is self-similar due to the absence of characteristic spatial scale. The key parameters for this problem are Mach number M of the shock (or oncoming gas flow), density ratio $\omega=\rho_T/\rho_0\neq 1$ and heat ratio $\gamma=1.4$.

If M is fixed, density ratio ω determines distinct flow regimes – regular and irregular. If ω is near unity, regular shock refraction takes place: all slightly distorted shocks and tangential discontinuities are conjugated in a single point.

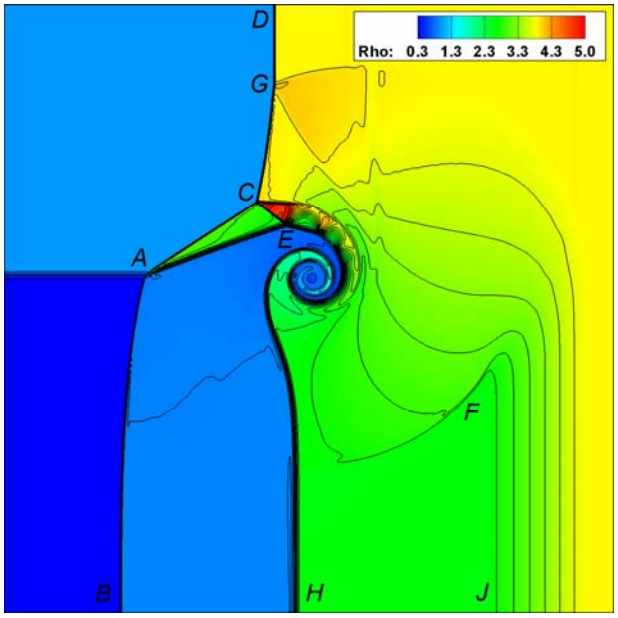

Fig. 2 An irregular interaction of a shock with quarter-plane density area: density contour for M = 3, $\omega = 0.3$

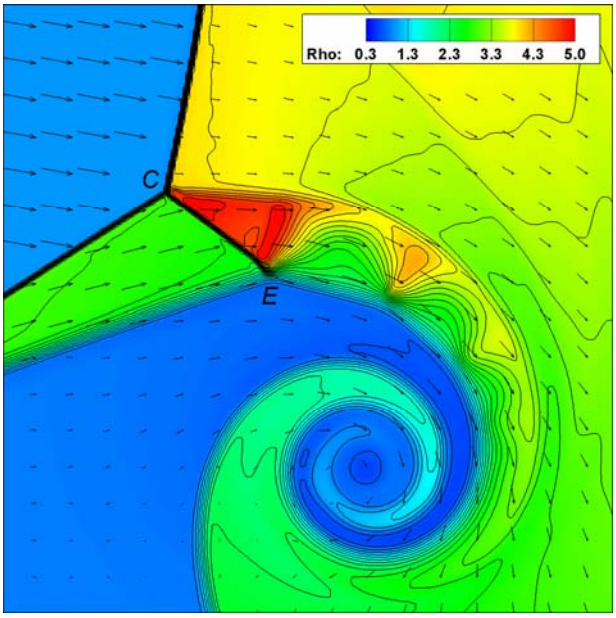

Fig. 3 The high-enthalpy stream and lamellar vortex structure.

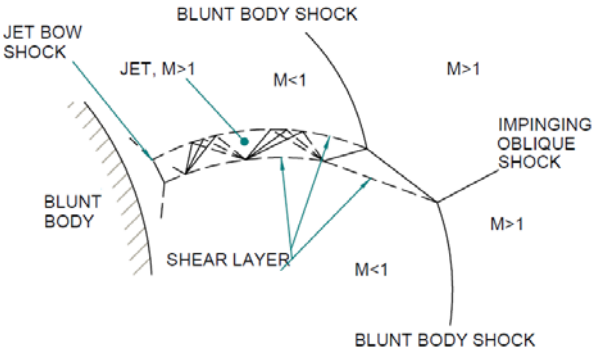

Fig. 4 Similar high-enthalpy stream structure for steady interaction of an oblique shock with a bow shock in front of a blunt body [14].

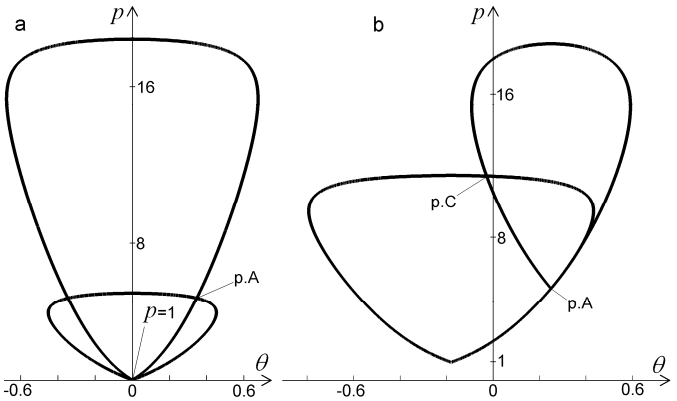

Fig. 5 Shock polar diagrams for point A (left) and point C (right), $M = 3, \omega = 0.3$.

The first irregular refraction regime takes place for $\omega < 0.8$: density contour for $M = 3, \omega = 0.3$ is shown at fig. 2. The bottom part of the flow is one-dimensional Riemann problem: leading shock B propagates to the left, rarefaction wave J – to the right, contact discontinuity H is in between. The undisturbed part DG of initial shock is situated at the top. The main flow area is occupied by complex shock structure, including oblique shock AC which connects leading and initial shocks, refracted shear layer AE and internal shock CE. A high-enthalpy gas stream is formed behind the internal shock; the stream turns down due to pressure difference at the lower and upper stream edges. A large-scale vortex and weak shock F are formed; propagation velocity of the latter is comparable with leading shock velocity. Being induced by interaction of initial and oblique shocks, initial shock distortion CD and triple point G formation take place.

The use of much more accurate computing grids than before has led to revealing of new quantitative flow features, such as complex high-enthalpy stream structure and lamination of the vortex (fig. 3, motion is relative to point C). Internal stream structure is formed by a set of unsteady Prandtl-Meyer-like compression-rarefaction wave fans, which are centered on the lower stream edge fractures and are reflected off the upper edge. The total pressure loss in the stream is much lower than elsewhere: at given parameters it equals 25% for gas passing shocks AC&CE and 67% for gas behind initial shock D. The vortex is formed by gas layers of different temperature $T = p/\rho$: "cold" gas comes from the stream and "hot" gas is captured from the area behind leading shock B. In whole, local flow presents an unsteady analogue for well-known Edney-IV shock interaction pattern [14] (fig. 4).

The length and angle of oblique shock AC is independent of Mach number M and is well approximated (up to 2-3% accuracy) by simple equation $\sin\alpha = \sqrt{\omega}$ [1], where α is the angle between AC and the horizontal axis.

Exact self-similarity of the flow has been observed in the numerical results. For an additional accuracy, most of the simulations were carried out using first-order Godunov scheme along with MacCormack method. Key flow features, such as positions and angles of shocks as long as gas parameters behind them, differed for less than 1%. Due to higher accuracy order, the MacCormack scheme provides much clearer shock and wave fan fronts. Slightly different pattern for interaction of CE shock with AE shear layer was observed due to significant blurring of the latter by the Godunov scheme.

"Semi-analytical" flow parameters estimation method It is possible to estimate main flow features, such as AC and CE shock angles along with gas parameters in the high-enthalpy stream, using shock polar method without direct flow simulation. The first part of algorithm deals with solving one-dimensional Riemann problem at the bottom flow area. The problem comes to a single algebraic equation which is solved for any accuracy by the Newton method. If the point A velocity is assumed to be equal to B shock velocity, a pair of shock polar diagrams may be drawn for the point (fig. 5a). The coordinates for the graph are the angle of flow turn θ and pressure p. The coordinates of curve intersection, which describes local flow near point A, are also found by algebraic equation solving. Gas state throughout whole ACE area is assumed uniform and equal to the state just behind AC shock near point A. The point C velocity is derived from AC shock velocity and angle, neglecting initial shock D distortion near the point. Then a pair of similar shock diagrams may be drawn for point C (fig. 5b), which leads to estimation of gas parameters behind the internal shock.

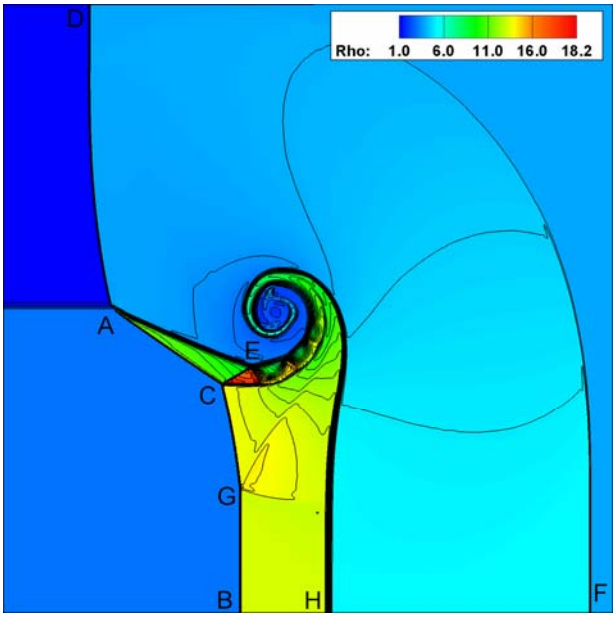

Fig. 6 An irregular shock-quarter-plane interaction pattern for $M = 3, \omega = 3$, density contour.

Comparison of these estimations with full simulation results for $M \in (1.5, 2.5)$ and $\omega \in (0.1, 0.5)$ shows that the method allows one to estimate high-enthalpy stream parameters up to 5-10% accuracy. If $M \geq 2$, such estimation of gas state in ACE area is better (<6% error) than simple estimation based on equation $\sin\alpha = \sqrt{\omega}$ (6-15% error).

Quarter-plane of "heavy" gas Another irregular shock refraction pattern takes place in case of $\omega > 1.1$. The density contour for $M = 3, \omega = 3$ is given at fig. 5. The one-dimensional Riemann problem at the bottom is of different kind: both B (transmitted) and F (reflected) waves are shocks, H is a contact discontinuity. The central shock structure is similar to $\omega < 0.8$ case: there is oblique shock AC which connects initial shock D with slow transmitted shock B and internal shock C. The high-enthalpy stream is formed by similar centered compression-rarefaction waves. Gas density behind internal shock CE $(\rho = 18.2)$ is more than $(\gamma+1)/(\gamma-1) = 6$ times higher that initial density in the quarter-plane $(\rho = 3)$. Thereby the density here reaches the value that is not attainable by compressing the gas with a single flat shock of any intensity. The angle of oblique shock AC is well approximated (<5% error) with similar equaton: $\sin\alpha = 1/\sqrt{\omega}$.

INTERACTION OF A SHOCK WITH THIN DENSITY LAYER The problem of interaction of a shock with a thin density layer is not self-similar due to presence of spatial scale – the layer width h. However, the latter determines only the time scale: exactly the same results (disregarding coordinates scale) may be obtained by computing the flow up to time moment t_1 for width value h_1 or up to moment $t_2 = t_1 \cdot h_2 / h_1$ for width value h_2.

For the case of $\omega \approx 1$ regular shock refraction patterns take place: initial shock slightly distorts and the width of the layer changes upon passing through the shock.

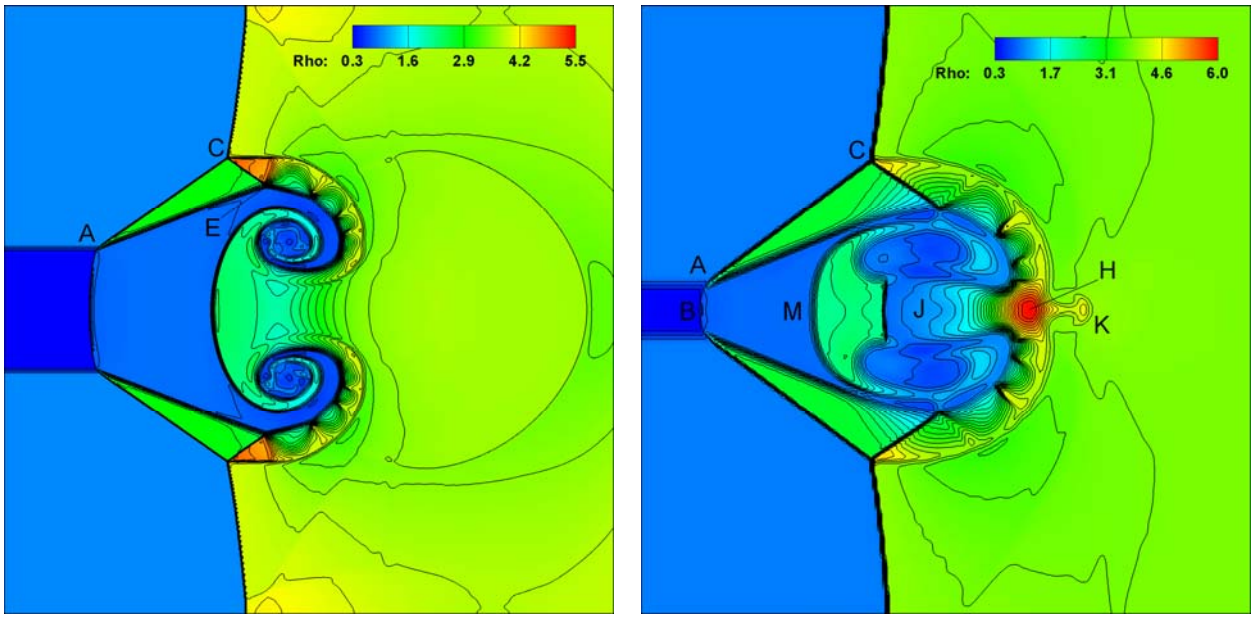

Fig. 7 An irregular refraction of a shock on a thin layer of light gas for $M = 2, \omega = 0.3$, same time moment for different layer widths: $h = 0.1$ (left), $h = 0.03$ (right). Plane flow, density contour.

The first irregular refraction pattern takes place for $\omega < 0.8$. An initial stage of the flow is quantitatively similar to a pair of quarter-plane problems (fig. 7, left). The forerunner consisting of a pair of oblique shocks AC, internal shocks CE, and high-enthalpy streams is formed. A mushroom-like reverse-flow vortex area is formed near the plane of symmetry. At later time moments (or at the same moment for lesser layer widths) an area H of high pressure and density is formed due to opposite flow of high-enthalpy streams (fig. 7, right). "Mushroom cap" M tears off and moves towards the leading shock B. Two gas streams flow from the H area: supersonic J stream moves towards the leading shock and weak K stream moves in the opposite direction. As well as high-enthalpy streams, J stream is supersonic relatively to the initial shock. Mushroom cap M is separated from the J stream by a shock.

The axisymmetric interaction of a shock with a thin channel of light gas is qualitatively the same, yet cumulation effect of opposite streams (which form one ring-shaped stream here) develops earlier. The area H of cumulation has slightly different structure: maximum pressure value is reached at the axis, while maximum-density area is of toroidal shape.

Detailed adaptive computational grids were used to simulate the flow for very thin layers at large time scales. Fig. 8 shows forerunner length d (which is the range between leading and initial shocks) dependence on time for different h. Straight line $h = 0.5$ represents infinitely wide layer, corresponding to one-dimensional Riemann

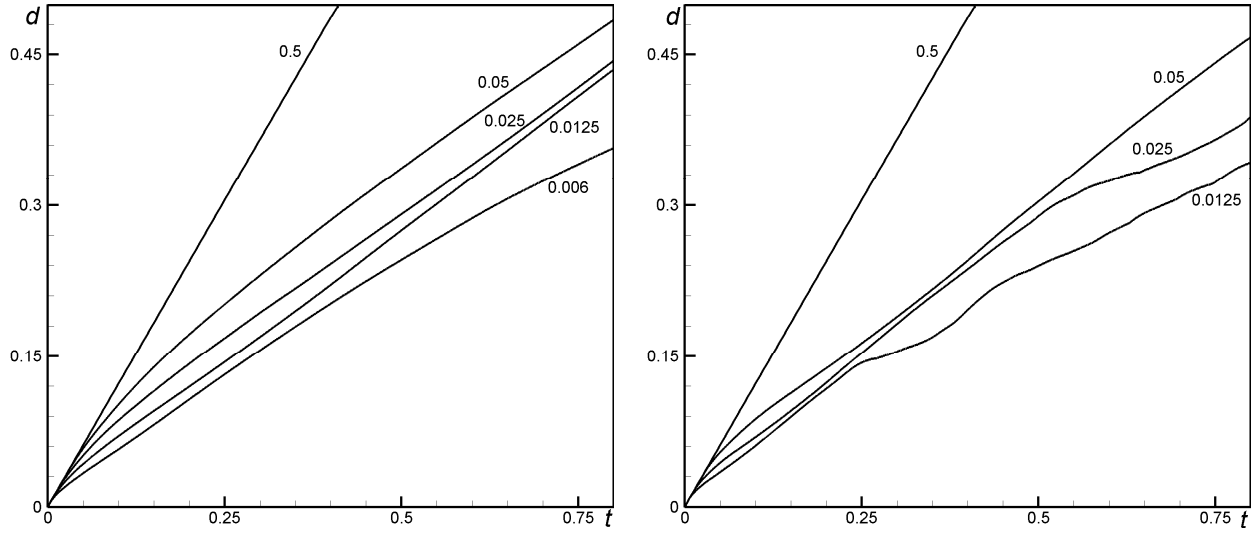

Fig. 8 The dependence of the forerunner length d on time for different h: plane (left) and axisymmetrical (right) flows. Width value $h = 0.5$ corresponds to infinitely wide layer – one-dimensional Riemann problem.

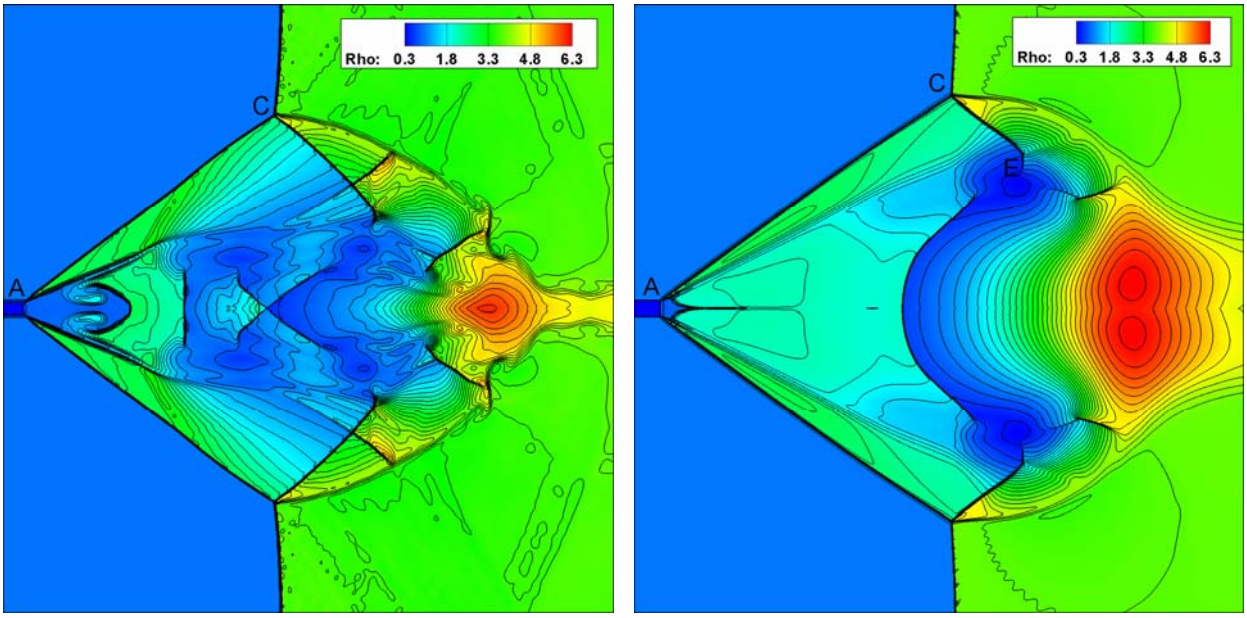

Fig. 9 The late flow stage computed by the MacCormack (left) and Godunov (right) methods.

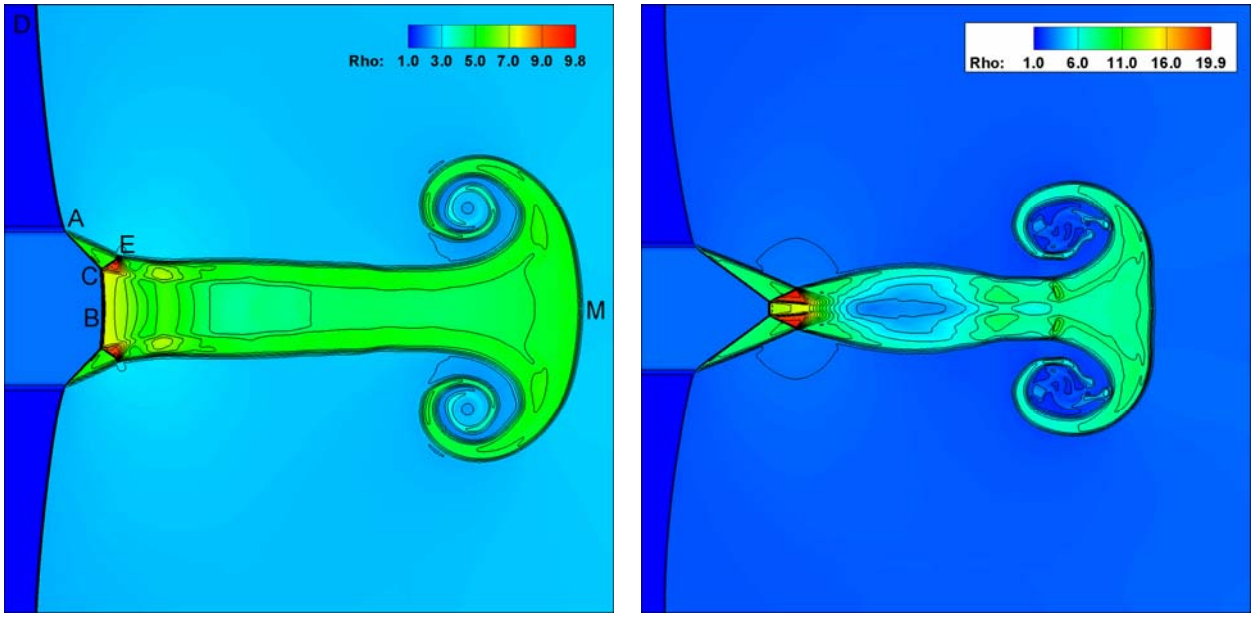

Fig. 10 Two irregular regimes for refraction of a shock on heavy gas layer for $M = 2$: $\omega = 2$ (left) and $\omega = 3$ (right).

problem.

For the certain time interval, forerunner growth rate is independent of h and is the same for plane and axisymmetrical flows: there are similar straight sections of the same slope on all curves. In this regard the layer width h determines only the time needed to reach the constant forerunner growth speed.

However, the linear forerunner growth law is disturbed at some moment (see $h = 0.006$ at fig. 8 left, and $h = 0.025, 0.0125$ at the right); the effect develops faster for axisymmetric case. Forerunner growth slowdown is caused by flow rearrangement behind its front: detached and distorted "mushroom cap" effectively chokes the flow behind the leading shock (fig. 9, left), so that complex vortical flow is developed. Simulation by the Godunov scheme (fig. 9, right) does not demonstrate such a complex internal flow, though the forerunner growth slowdown rate is the same.

Thin layer of "heavy" gas For the case of "heavy" gas layer two distinct irregular refraction patterns were found depending on density ratio ω. Fig. 10 left, demonstrates the density contour for the first regime at $M = 2, \omega = 2$. A pair of triangle shock structures ACE and a mushroom-like gas stream are formed. The stream is lamellar: gas velocity behind the internal shocks CE is greater than velocity behind the transmitted shock B. The gas right behind the transmitted shock has subsonic velocity relative to initial shock D, but accelerates to supersonic speed in the rarefaction wave. The overall flow structure remains the same as the time passes: the stream passes further behind the shock and retains width constant.

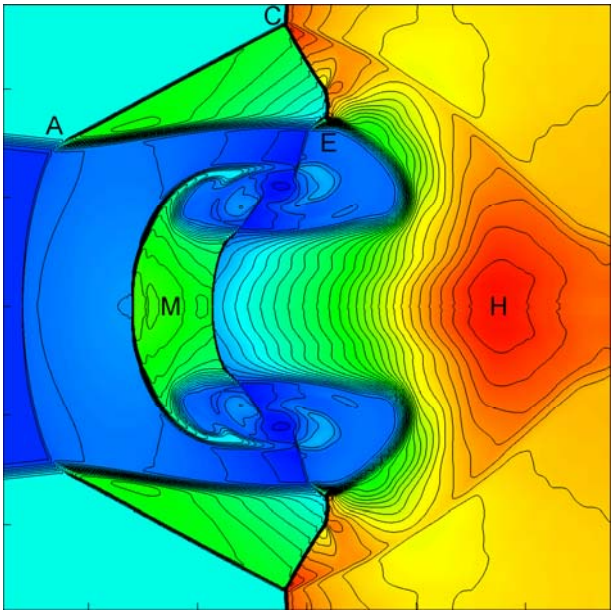

Fig. 11 Very thin light gas wedge: $\beta/2 = 5^o$

The other flow type is formed for $M = 2, \omega = 3$ (fig. 10, right). The stream is barrel-shaped and the number of barrels increases as the stream propagates behind the shock. Thus a locally steady flow, analogous to classic problem of over-expanded stream outflow is formed. Axisymmetrical flow has qualitatively similar overall structure.

INTERACTION OF A SHOCK WITH "DENSITY WEDGE" The problem of interaction of a shock with gas "density wedge" (III at fig. 1) is self-similar; Key parameters are M, ω, γ, wedge inclination angle α and wedge apex angle β. The α is the angle between horizontal axis and the wedge symmetry plane. Both $\alpha = 0$ ("symmetrical wedge") and $\alpha > 0$ ("asymmetrical wedge")

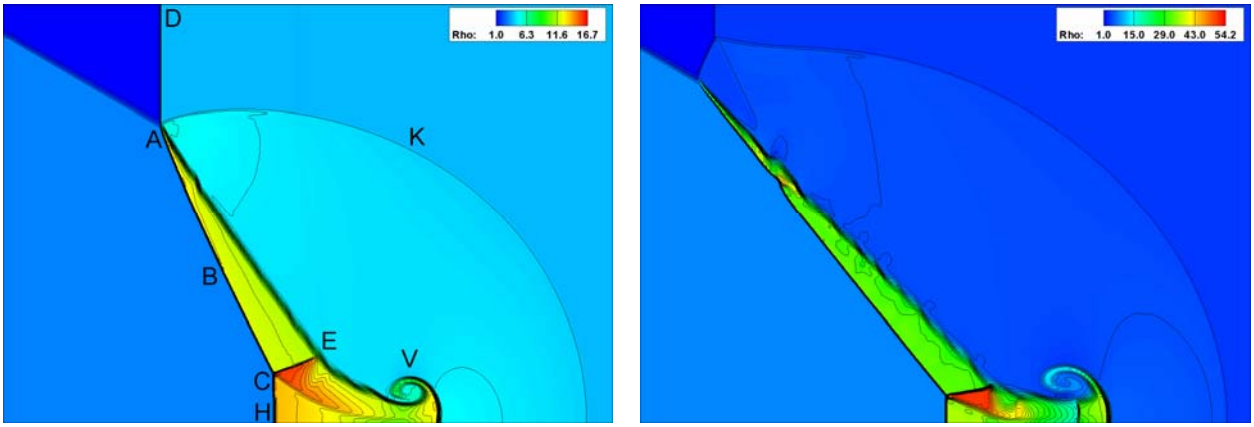

Fig. 12 Non-regular shock refraction patterns for "heavy gas wedge" at $M=3, \alpha=0, \beta/2=30^o$: irregular (left, $\omega=3$), mach (right, $\omega=8$)

cases were considered. For the symmetrical case, if $\omega \approx 1$ or β is large enough, the regular shock refraction patterns occur [2-3]: all the shocks and tangential discontinuities have nearly flat surfaces and are conjugated in the single point.

Symmetrical wedge of "light" gas Local shock refraction patterns at inclined slow-fast gas interface are well-known [2] and are not presented in this paper. The difference introduced by the presence of wedge apex consists of formation of mushroom-like vortex area near the former. It is significant in the case of very small apex angle: the flow structure (fig. 11) is quantitatively similar to the forerunner structure (fig. 7). The similar effects of opposite streams cumulation (area H) and "mushroom cap" M detaching take place. However, there is no flow choking phenomenon due to self-similar expansion of the whole structure.

Symmetrical wedge of "heavy" gas Non-regular shock refraction patterns for $\alpha=0, \omega>1$ (fast-slow gas interface) are shown at fig. 12. For irregular regime (fig. 12, left) there is a single conjunction point A for the initial shock D, transmitted shock B, reflected shock K and refracted tangential discontinuity AE. Mushroom-like vortex structure V is formed near the wedge apex. The transmitted shock B undergoes the mach reflection off the symmetry plane: triple point C and mach stem H are formed. Distinctive mach "nozzle" develops behind the stem and its width diminishes to zero at some point. The latter effect takes place due to flow self-similarity: gas does not outflow from the nozzle but is accumulated inside it while the mach stem grows and propagates to the left. This refraction pattern is retained for lesser apex angle values; for $\beta \le 5^o$ an analogy with the refraction of a shock on a thin heavy gas layer (fig. 10, right) occurs: a set of self-similar expanding barrel-like structures is formed near the plane of symmetry.

For the same parameter values $M=3, \beta/2=30^o$ and significantly higher density ratio ($\omega=8$), the mach refraction pattern takes place (fig. 12, right). It is characterized not only by formation of a mach stem AG between initial and transmitted shock, but additionally by the separation of "mushroom cap" of vortex area near the symmetry plane.

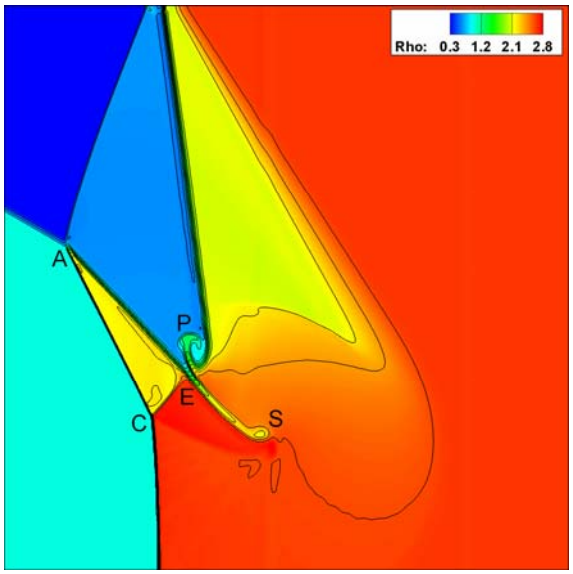

Fig. 14 Strongly inclined wedge: $\alpha=45^o$, $\beta=30^o$

Asymmetrical wedge of "light" gas. If the wedge is asymmetrical but the inclination angle is not excessive ($0<\alpha\le\beta/2$), the flow corresponds to a pair of refraction patterns observed for the symmetrical cases: local shock patterns are exactly the same, and asymmetry has significant effect only at mushroom-like vortex area warping.

If the wedge is thin enough and is strongly inclined ($\alpha>\beta/2$), another flow type takes place. Two slipping streams P and S are formed near the wedge apex (fig. 13). The regular shock refraction takes place at the top area: all wave surfaces are conjugated in a single point. The lower part of the flow is some analogue for shock refraction on a quarter-plane density area: forerunner-like triangle shock structure ACE is formed. The stream slipping effect is more intense for higher α and lower β values.

INTERACTION OF A SHOCK WITH ELLIPTIC GAS BUBBLE The key parameters for the problem of interaction of a shock with elliptic (axisymmetrical flow) or cylindrical (plane flow) gas bubble (IV at fig. 1) are the M, ω, γ and the axle lengths a, b. The regular interaction takes place in case of $\omega \approx 1$: the shock slightly distorts during the transition through bubble and the latter retains nearly elliptic shape, compressed along the x axis. Undisturbed and transmitted parts of the shock are connected at the single point on the bubble edge.

"Light" elliptic gas bubble An irregular refraction for the case of $\omega < 1$ is characterized by a set of non-linear features. As the time passes, different conjunction regimes for the initial shock B, leading shock C and bubble edge A take place (fig. 15): the regular, irregular and twin mach. The reflected shock E, hanging shock F and baroclinic vortex V are formed. While transmitted shock passes through the opposite (left) edge of the bubble, reflected cumulative shock P is formed (fig. 16). Lower part of its surface moves to the right and the upper part moves towards the symmetry axis, so that shock is gradually "tumbles" (fig. 16, right). This process leads to formation of triple point and a secondary cumulative shock Q. The triple point eventually reaches symmetry axis which result in local pressure and density rise – shock cumulation. There are two distinct cumulation regimes depending on the initial bubble elongation $e = a/b$: extremal gas state may be localized inside or outside the distorted bubble (dark blue area at fig. 16). In particular case of $M = 2, \omega = 0.3$ the internal and external cumulation regimes take place for $a > b$ and $a < b$ correspondingly. The most intensive pressure and density rise (see fig. 18 below) is observed for transitional cumulation regime, when the triple point reaches the symmetry axis at the position of contact discontinuity D.

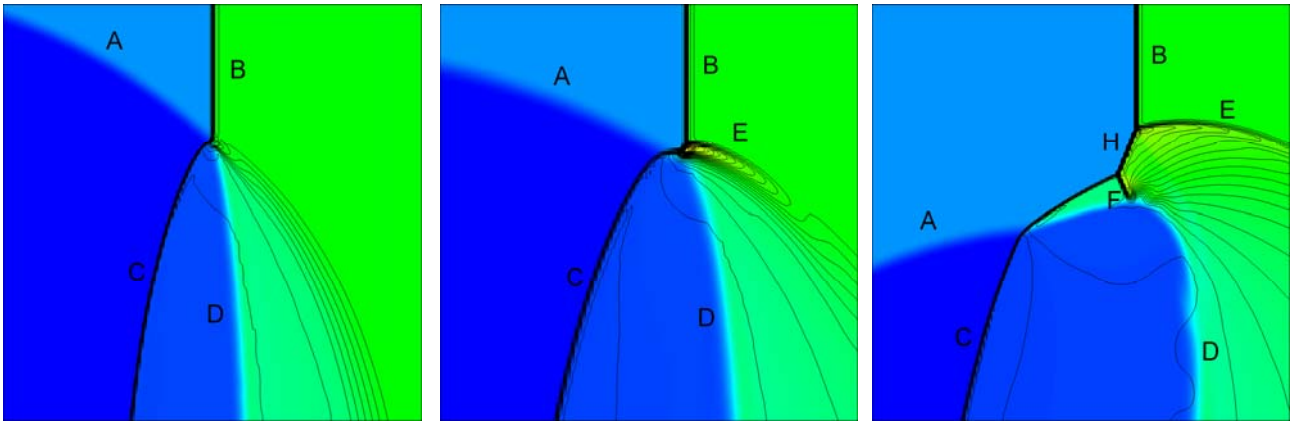

Fig. 15 The consecutive stages of shock refraction patterns for interaction of a shock with light gas bubble at $M = 2, \omega = 0.3, a = b = 0.2$: regular (left), irregular (center) and twin mach (right). Density coloring, pressure contour.

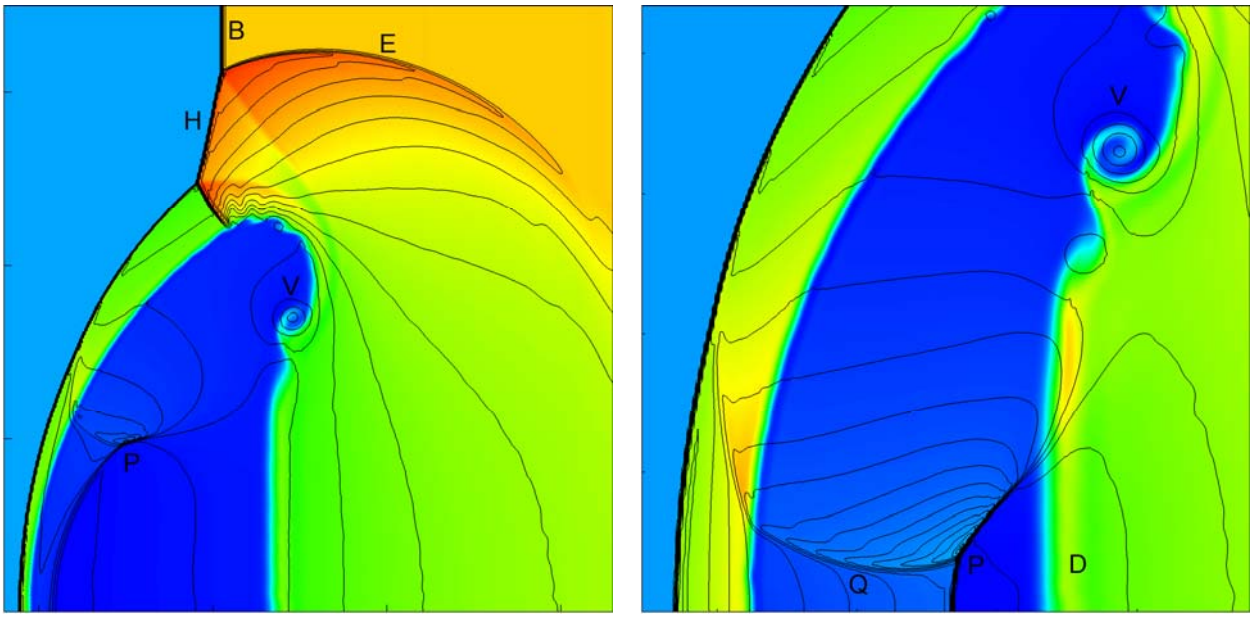

Fig. 16 Cumulative shock P propagation and tumbling for a shock-bubble interaction: $M = 2, \omega = 0.3, a = b = 0.2$, density coloring, pressure contour.

"Heavy" elliptic gas bubble The cumulation effect is present for the case of $\omega > 1$ as well, however the mechanism of the process is different. The arched reflected shock E is formed upon shock transition along with a chain of baroclinic vortices F; initial shock B is conjugated with transmitted shock C at the single point. Transmitted shock C has lesser propagation velocity than initial shock B, which rounds the bubble on the outside (fig. 17, left). Similarly to shock P at fig. 16, parts C1 and C2 of the transmitted shock C converge and form a triple point. Depending on bubble elongation e, different cumulation regimes were observed: part C1 of the transmitted shock may reach an opposite bubble edge after the initial shock fully rounds the bubble or before the moment. The former case – an internal cumulation – takes place for prolate bubbles ($e = a/b > 1$) and is shown at fig. 17 right ($a = 0.2, b = 0.1$); the directions of shocks C1 and C2 propagation are shown by arrows. The latter case – external cumulation – takes place for flattened bubbles ($e < 1$). In this case the triple point reaches the symmetry axis in an undisturbed gas area ahead of distorted bubble. For the case of $a = b$ the second triple point formation at shock C1 and more complex transitional cumulation process were observed.

The cumulation parameters, i.e. maximum gas parameters observed throughout the whole process of shock-bubble interaction, are shown at fig. 18 for different Mach numbers and bubble elongation are shown. Adaptive computational grids were used for accurate cumulation process resolving. The actual cumulation values were dependent on grid resolution: the pressure indefinitely increased as grid became more detailed. This effect is caused by the similarity between the flow and Huderley-type problems: the pressure of inviscid gas is infinite at the cumulation moment. Nevertheless, if grid resolution is fixed, it is possible to determine quantitative dependency of cumulation parameters on bubble elongation.

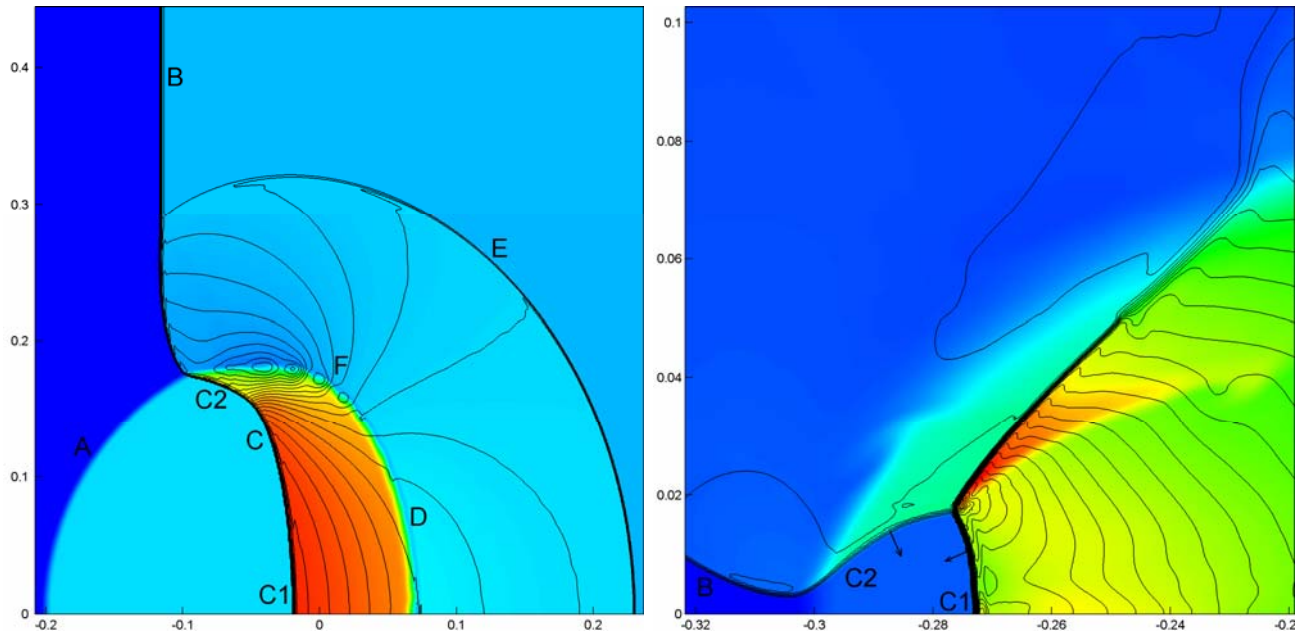

Fig. 17 Interaction of a shock with "heavy gas bubble", $M = 2, \omega = 3$: density coloring, pressure contour. Propagation and "tumbling" of transmitted shock C (left, $a = b = 0.2$), internal cumulation process (right, $a = 0.2, b = 0.1$).

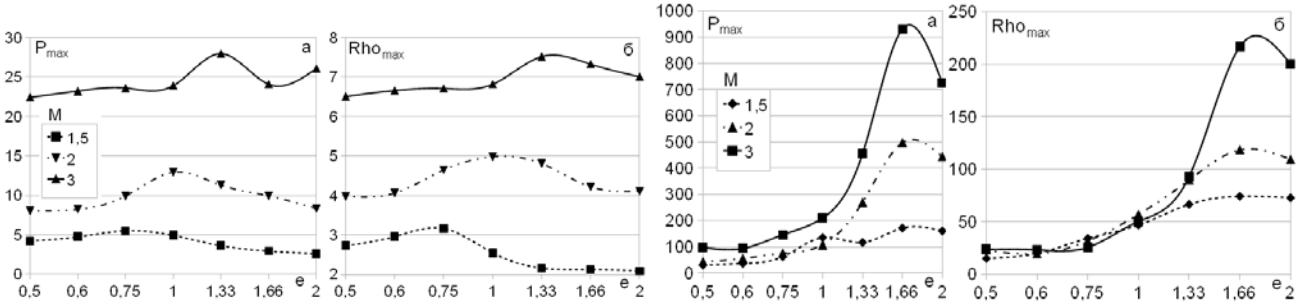

Fig. 18 Maximum pressure and density observed for interaction of a shock with light (left, $\omega = 0.3$) and heavy (right, $\omega = 3$) elliptic bubbles for $M = 1.5, 2, 3$ and $0.5 < e < 2$. Axisymmetric flow, symbols represent actual simulations for (M, e) pairs. Lines are interpolative curves.

The most intensive, transitional cumulation for light bubble takes place at different elongation values (fig. 18, left) for different Mach numbers: see $e = 0.75, 1, 1.33$ for $M = 1.5, 2, 3$ correspondingly. The extremely intensive internal cumulation for heavy bubble case takes place at $e = 1.66$ independently of Mach number (fig. 18, right).

The plane flows corresponding to cylindrical "bubbles" have a full set of the same quantitative features, though the cumulation process is less intensive.

Conclusion A set of problems of interaction of a plane shock with density inhomogeneities was considered. The new quantitative features of the flow, such as wave-structured high-enthalpy stream and lamellar vortex were found for the quarter-plane case. Typical forerunner structure growth was investigated, new regularities including its slowdown at late stages were revealed. Two distinct refraction regimes, including periodical barrel-like stream formation, were found for the case of thin layer of heavy gas. The new features of the flow for interaction of a shock with "gas wedge" were found, including a forerunner-like structure for very thin light wedge, complex shock reflection patterns near the symmetry plane of heavy wedge and a pair of slipping streams for thin inclined wedge. The details of shock cumulation process during the interaction of a shock with elliptic bubbles were identified; distinct cumulation regimes – internal and external, – depending on bubble elongation, were classified. The qualitative dependency of cumulation intensity on the shock intensity and bubble elongation was revealed, most intensive cumulation regimes was found.

Acknowledgments The present research is financially supported by Russian Foundation for Basic Research (grant 08-01-00033) and Russian Federal Agency on Science and Innovations (grant NSh-8424.2010.1).

References

1. Artem'ev, V.I., Bergel'son, V.I., Kalmykov, A.A., Nemchinov, I.V., Orlova, T.I., Rybakov, V.A., Smirnov, V.A., Khazins,V.M. *Development of a Forerunner in Interaction of a Shock Wave with a Layer of Reduced Density.* Fluid Dynamics, Vol. 23, No. 2, 1988, pp. 290–295.
2. A.M. Abf-el-Fattah, L.F. Henderson *Shock waves at a slow-fast gas interface*. Journal of Fluid Mechanics. 1978. V.86. pp. 79-95.
3. A.M. Abf-el-Fattah, L.F. Henderson *Shock waves at a fast-slow gas interface*. Journal of Fluid Mechanics. 1978. V.86. pp. 15-32.
4. Voinovich, P.A., Zhmakin, A.I., Fursenko, A.A. *Modeling of the Interaction of Shock Waves in Gases with Space Inhomogeneities of Parameters.* Journal of Technical Physics, Vol. 58, No. 7, 1988, pp. 1259–1267.
5. V.A. Andrushchenko, L.A. Chudov *Interaction between a plane shock wave and a spherical volume of hot gas*, Fluid Dynamics, Vol. 23, No. 1, 1988, pp. 78-82.
6. D. Ranjan, J. Niederhaus, J.G. Oakley, M.H. Anderson, R. Bonazza, J.A. Greenough *Shock-bubble interactions: Features of divergent shock-refraction geometry observed in experiments and simulations.* Physics of Fluids. 2008. V.20.
7. E. Schulein, A.A. Zheltovodov, E.A. Pimonov, M.S. Loginov *Experimental and Numerical Modeling of the Bow Shock Interaction with Pulse-Heated Air Bubbles.* International Journal of Aerospace Innovations. 2010. V.2. №3. pp. 165-187.
8. P.Yu. Georgievskii, V.A. Levin *Unsteady interaction of a sphere with atmospheric temperature inhomogeneity at supersonic speed*. Fluid Dynamics, Vol. 28, No. 4, 1993, pp. 568-574.
9. J.M. Picone, J.P. Boris *Vorticity generation by shock propagation through bubbles in a gas.* Journal of Fluid Mechanics. 1988. V.189. pp. 23-51.
10. P.Yu. Georgievskii, V.A. Levin and O. G. Sutyrin *Two-dimensional self-similar flows generated by the interaction between a shock and low-density gas regions.* Fluid Dynamics, 2010, 45 (2), pp. 281-288
11. P.Yu. Georgievskii, V.A. Levin and O. G. Sutyrin *Cumulation effect upon the interaction between a shock and a local gas region with elevated or lowered density.* Fluid Dynamics, 2011, 46 (6), pp. 967-974
12. MacCormack, R.W., *The Effect of Viscosity in Hypervelocity Impact Cratering.* AIAA Paper 1969-354, 1969.
13. V.P. Goloviznin, A.I. Zhmakin, A.A. Fursenko *On a method for calculating non-stationary interactions of shock waves.* Zh. vychisl. Mat. mat. Fiz. 1982. V.22. №2. pp. 480–484
14. Adelgren R.G., Elliot G.S., Knight D.D., Zheltovodov A.A., Beutner T.J. *Localized Flow Control in Supersonic Flow.* Proceedings of the 3rd Workshop on Magneto-Plasma Aerodynamics in Aerospace Applications. Ed. By V.A. Bityurin, Moscow, IVTAN, 2001, pp. 116-120